[11] T. Ducrocq, M. Hauspie, N. Mitton, and S. Pizzi, "On the impact of network topology on wireless sensor networks performances illustration with geographic routing," in *Proc. Int. Workshop PAEWN*, Victoria, BC, Canada, May 2014, pp. 1–6. [Online]. Available: http://hal.inria.fr/hal-00959921
[12] Univ. Calif. Berkeley, Motescope. [Online]. Available: http://smote.cs.berkeley.edu/motescope/
[13] R. Lim *et al.*, "FlockLab: A testbed for distributed, synchronized tracing and profiling of wireless embedded systems," in *Proc. 12th Int. Conf. Inf. Process. Sensor Netw.*, 2013, pp. 153–166.
[14] R. N. Murty *et al.*, "CitySense: An urban-scale wireless sensor network and testbed," in *Proc. IEEE Conf. Technol. Homeland Security*, 2008, pp. 583–588.
[15] I. Corredor, A. García, J. Martínez, and P. López, "Wireless sensor network-based system for measuring and monitoring road traffic," in *Proc. 6th CollECTeR*, Madrid, Spain, Jun. 2008.
[16] J. Hu, J. Song, M. Zhang, and X. Kang, "Topology optimization for urban traffic sensor network," *Tsinghua Sci. Technol.*, vol. 13, no. 2, pp. 229–236, Apr. 2008.
[17] X. Mao, X. Miao, Y. He, X.-Y. Li, and Y. Liu, "CitySee: Urban CO2 monitoring with sensors," in *Proc. IEEE INFOCOM*, 2012, pp. 1611–1619.
[18] S. Faye, C. Chaudet, and I. Demeure, "Influence of radio communications on multiple intersection control by a wireless sensor network," in *Proc. 13th ITST*, 2013, pp. 307–312.
[19] S. Porta, P. Crucitti, and V. Latora, "The network analysis of urban streets: A primal approach," *Environ. Planning B, Planning Des.*, vol. 33, no. 5, pp. 705–, 2006.
[20] P. Crucitti, V. Latora, and S. Porta, "Centrality measures in spatial networks of urban streets," *Phys. Rev. E, Stat. Nonlinear, Soft Matter Phys.*, vol. 73, no. 3, Mar. 2006, Art. ID. 036125.
[21] S. Porta, P. Crucitti, and V. Latora, "The network analysis of urban streets: A dual approach," *Phys. A, Stat. Mech. Appl.*, vol. 369, no. 2, pp. 853–866, Sep. 2006.
[22] D. Naboulsi and M. Fiore, "On the instantaneous topology of a large-scale urban vehicular network: The Cologne case," in *Proc. 14th ACM Int. Symp. Mobile Ad Hoc Netw. Comput.*, 2013, pp. 167–176.
[23] M. Tubaishat, Q. Qi, Y. Shang, and H. Shi, "Wireless sensor-based traffic light control," in *Proc. 5th IEEE CCNC*, Las Vegas, NV, USA, Feb. 2008, pp. 702–706.
[24] A. Haoui, R. Kavaler, and P. Varaiya, "Wireless magnetic sensors for traffic surveillance," *Transp. Res. C, Emerging Technol.*, vol. 16, no. 3, pp. 294–306, Jun. 2008.
[25] *Coexistence of Wireless Personal Area Networks With Other Wireless Devices Operating in Unlicensed Frequency Bands*, IEEE Std. 802.15.2-2003, 2003.
[26] K. Marquess, "Physical model sub-group discussion and questions," CETECOM Inc., Fremont, CA , USA, IEEE 802.15/138R0, 1999.
[27] M. Haklay, "How good is volunteered geographical information? A comparative study of OpenStreetMap and ordnance survey datasets," *Environ. Planning B, Planning Des.*, vol. 37, no. 4, pp. 682–703, 2010.
[28] D. Krajzewicz, J. Erdmann, M. Behrisch, and L. Bieker, "Recent development and applications of SUMO—Simulation of urban mobility," *Int. J. Adv. Syst. Meas.*, vol. 5, no. 3/4, pp. 128–138, Dec. 2012. [Online]. Available: http://elib.dlr.de/80483/
[29] E. N. Gilbert, "Random graphs," *Ann. Math. Statist.*, vol. 30, no. 4, pp. 1141–1144, Dec. 1959.
[30] P. Erdös and A. Rényi, "On random graphs I," *Publicationes Math.*, vol. 6, pp. 290–297, 1959.
[31] M. Penrose, *Random Geometric Graphs*. London, U.K.: Oxford Univ. Press, 2003, ser. Oxford Studies in Probability.
[32] A.-L. Barabási and R. Albert, "Emergence of scaling in random networks," *Science*, vol. 286, no. 5439, pp. 509–512, Oct. 1999.
[33] D. J. Watts and S. H. Strogatz, "Collective dynamics of "small-world" networks," *Nature*, vol. 393, no. 6684, pp. 440–442, Jun. 1998.
[34] M. Molloy and B. Reed, "A critical point for random graphs with a given degree sequence," *Random Struct. Algorithms*, vol. 6, no. 2/3, pp. 161–180, Mar.–May 1995.

BER Performance of Spatial Modulation Systems Under 3-D V2V MIMO Channel Models

Yu Fu, Cheng-Xiang Wang, *Senior Member, IEEE*, Yi Yuan, Raed Mesleh, *Senior Member, IEEE*, el-Hadi M. Aggoune, *Senior Member, IEEE*, Mohammed M. Alwakeel, *Senior Member, IEEE*, and Harald Haas, *Member, IEEE*

***Abstract*—In this paper, the bit error rate (BER) performance of spatial modulation (SM) systems under a novel 3-D vehicle-to-vehicle (V2V) multiple-input multiple-output (MIMO) channel model is investigated both theoretically and by simulations. The impact of vehicle traffic density, Doppler effect, and 3-D and 2-D V2V MIMO channel models on the BER performance are thoroughly investigated. Simulation results show that the performance of SM is mainly affected by the spatial correlation of the underlying channel model. Compared with other MIMO technologies, the SM system can offer a better tradeoff between spectral efficiency and system complexity.**

***Index Terms*—Bit error rate (BER), spatial diversity, spatial modulation (SM), spatial multiplexing, 3-D vehicle-to-vehicle (V2V) multiple-input multiple-output (MIMO) channel models.**

I. Introduction

Over the past few decades, multiple-input multiple-output (MIMO) technologies have been widely used to obtain high data rates and increase spectral efficiency [1]. However, existing MIMO technologies suffer from various problems, such as the interchannel interference (ICI), limited spectral efficiency, and high complexity of the system [2]. In recent years, another MIMO technology called spatial modulation (SM) has attracted much research interest due to its enhancement of spectral efficiency and reasonable system complexity [2], [3]. The basic idea for SM is that, at each time instant, only one antenna

Manuscript received May 18, 2014; revised November 7, 2014 and March 13, 2015; accepted June 30, 2015. Date of publication July 28, 2015; date of current version July 14, 2016. This work was supported in part by the SNCS Research Center, University of Tabuk, Ministry of Higher Education in Saudi Arabia, by the EU FP7 QUICK Project PIRSES-GA-2013-612652, by the EU H2020 ITN 5G Wireless Project 641985, by the Ministry of Science and Technology in China International Science and Technology Cooperation Program under Grant 2014DFA11640, by 863 project in 5G under Grant 2014AA01A707, and by the UK Engineering and Physical Sciences Research Council (EPSRC) under Fellowship Grant EP/K008757/1. The review of this paper was coordinated by Prof. Y. Gong. *(Corresponding author: Cheng-Xiang Wang.)*

Y. Fu and Y. Yuan are with the Institute of Sensors, Signals and Systems, School of Engineering and Physical Sciences, Heriot-Watt University, Edinburgh EH14 4AS, U.K. (e-mail: yf54@hw.ac.uk; yyuan1116@gmail.com).

C.-X. Wang is with the Institute of Sensors, Signals and Systems, School of Engineering and Physical Sciences, Heriot-Watt University, Edinburgh EH14 4AS, U.K., with the School of Information Science and Engineering, Shandong University, Jinan 250100, China and also with the SNCS Research Center, University of Tabuk, Tabuk 71491, Saudi Arabia (e-mail: cheng-xiang.wang@hw.ac.uk).

R. Mesleh, e.-H. M. Aggoune, and M. M. Alwakeel are with the SNCS Research Center, University of Tabuk, Tabuk 71491, Saudi Arabia (e-mail: raed.mesleh@ieee.org; haggoune.sncs@ut.edu.sa; alwakeel@ut.edu.sa).

H. Haas is with the Joint Research Institute for Signal and Image Processing, Institute for Digital Communications, University of Edinburgh, Edinburgh EH9 3JL, U.K. (e-mail: h.haas@ed.ac.uk).

Color versions of one or more of the figures in this paper are available online at http://ieeexplore.ieee.org.

Digital Object Identifier 10.1109/TVT.2015.2461638

is active. The index of the active antenna becomes a resource for carrying information. Benefiting from this extra resource, SM can obtain relatively high spectral efficiency with low-order modulation schemes [2]. Moreover, as only one antenna is used to transmit at each time instant, the ICI problem is entirely avoided, and simple receiver algorithms can be employed [4], [5].

Vehicle-to-vehicle (V2V) communication has been a hot research topic in recent years [6]. With multiple antennas equipped on the vehicle, MIMO technologies such as SM can be widely used by V2V communications for safety device communications, ad hoc peer-to-peer networks, and intelligent transportation systems [6], [7]. Compared with traditional fix-to-mobile (F2M) communications, the biggest challenge in V2V communications is the severe environment caused by the fast movement of both the transmitter (Tx) and the receiver (Rx). To design and test V2V communication technologies, channel models that can accurately represent the propagation characteristics of V2V communication environments should be developed [8], [9]. In [7], a novel 3-D V2V geometry-based stochastic channel model (GBSM) has been proposed, which is the first 3-D V2V channel model that can accurately capture the effect of vehicular traffic density (VTD) on the channel.

The bit error rate (BER) performance of SM has, so far, been mainly investigated for some simple F2M channels, such as Rayleigh, Rician, and Nakagami fading channels [2], [4], [5], [10], and some measured channels of simple indoor environments [11]–[13]. In [14], the BER performance of SM systems was first studied under a simple 2-D V2V MIMO channel model [15], [16] but only contained double bounced (DB) components. To the best of the authors' knowledge, there is no relevant study on the performance of SM systems under more realistic 3-D V2V MIMO channel models. To fulfill the research gap, this paper investigates the BER performance of SM systems using the 3-D V2V MIMO channel model in [7] with different VTD scenarios and system settings.

The major contributions of this paper are summarized as follows. First, we derive a tight closed-form upper bound of the theoretical average BER (ABER) of SM systems under a novel 3-D narrowband V2V GBSM. Second, the impact of different realistic issues, such as VTD scenarios and the speed of vehicles represented by Doppler shift, on channel statistic properties and the BER performance of SM systems are thoroughly investigated. Third, the BER performance of SM systems is compared with that of other MIMO technologies (spatial diversity and spatial multiplexing) under the realistic 3-D V2V channel model. To the best of the authors' knowledge, the aforementioned aspects have yet to be studied.

The remainder of this paper is organized as follows. In Section II, a review of SM is given. In Section III, the 3-D V2V MIMO channel model and some important statistical properties are described. The theoretical expression of the ABER for SM under the 3-D V2V MIMO channel model is derived in Section IV. In Section V, numerical and simulation results are presented and analyzed. Finally, conclusions are given in Section VI.

II. Spatial Modulation Systems

Compared with other MIMO technologies, the most unique characteristic in SM is that only one antenna is used to transmit data at each time instant, and antenna indexes are used to carry information [2]. Let us assume an SM system with N_t transmitters and N_r receivers, the M quadrature amplitude modulation/phase-shift keying (PSK) modulation scheme is used as the digital modulator. The bit stream is divided into two parts: The first $\log_2(N_t)$ bits are carried by the antenna index and used for antenna selection. The other $\log_2(M)$ bits are transmitted through the digital modulated symbol. Thus, at each time instant, $m = \log_2(N_t) + \log_2(M)$ bits are transmitted, where m is the spectral efficiency of the SM system in bits per symbol.

Let $\boldsymbol{S}$ denote the $N_t \times 1$ transmit vector at the Tx side. At each time instant, as there is only one Tx antenna active, $\boldsymbol{S}$ can be further expressed as $\boldsymbol{S} = [0, 0, \ldots, S, \ldots, 0, 0]^T_{N_t}$, where $[.]^T$ denotes transpose operation. At the Rx, the received $N_r \times 1$ vector $\boldsymbol{y}(t)$ can be written as

$$\boldsymbol{y}(t) = \boldsymbol{H}(t, \tau) \otimes \boldsymbol{S}(t) + \boldsymbol{N} \tag{1}$$

where $\otimes$ denotes convolution, $\boldsymbol{N}$ is the $N_r \times 1$ complex additive white Gaussian noise vector, with real and imaginary parts, both having a double-sided power spectral density that is equal to $N_0/2$ [2]. In addition, $\boldsymbol{H}(\boldsymbol{t}, \boldsymbol{\tau})$ is the $N_r \times N_t$ channel matrix, which is composed of $h_{q,p}(t, \tau), p = 1, \ldots, N_t,\ q = 1, \ldots, N_r$. Here, $h_{q,p}(t, \tau)$ is the channel impulse response between the pth Tx and the qth Rx at time t and with delay τ.

In our system, the Tx and the Rx are assumed to have perfect synchronization in both time and frequency. Full channel state information is available at the Rx. The task of the receiver is to jointly estimate the index of the active transmit antenna and the modulation symbol at this particular time instant. The optimum maximum likelihood (ML) detector proposed in [4] is employed to estimate the transmit antenna index $\hat{p}$ and the transmitted data symbol $\hat{s}$ as

$$\begin{aligned}[\hat{p}, \hat{k}] &= \arg\min_{p,k} \left(\|y - H \otimes S_k\|^2_F \right) \\ & p \in \{1 : N_T\} \text{ and } k \in \{1 : M\}\end{aligned} \tag{2}$$

where $\| \cdot \|_F$ denotes the Frobenius norm.

III. 3-D Vehicle-To-Vehicle Multiple-Input Multiple-Output Channel Model

In this paper, the narrowband 3-D V2V MIMO channel model proposed in [7] is used to test the BER performance of SM systems. For this model, the propagation environment consists of both line-of-sight (LoS) and non-LoS components, which can further be classified as single bounced (SB) rays representing signals reflected only once during the propagation process and DB rays representing signals reflected more than once. In this channel model, the stationary scatters such as buildings are abstracted as an elliptic cylinder, and moving scatters, such as other vehicles, are abstracted and located on two spheres around the Tx and the Rx.

For the 3-D channel model, each element $h_{q,p}(t)$ contains three types of components, namely, the LoS component, SB components, and DB components, which can be expressed as

$$h_{q,p}(t) = h^{\mathrm{LoS}}_{qp}(t) + \sum_{i=1}^{I} h^{\mathrm{SB}_i}_{qp}(t) + h^{\mathrm{DB}}_{q,p}(t) \tag{3}$$

$$\begin{aligned}h^{\mathrm{LoS}}_{q,p}(t) = \sqrt{\frac{K}{K+1}} & e^{-j2\pi f_c \tau_{qp}} \times e^{j2\pi f_{T\max} t \cos\left(\alpha^{\mathrm{LoS}}_T - \gamma_T\right) \cos \beta^{\mathrm{LoS}}_T} \\ & \times e^{j2\pi f_{R\max} t \cos\left(\alpha^{\mathrm{LoS}}_R - \gamma_R\right) \cos \beta^{\mathrm{LoS}}_R}\end{aligned} \tag{4a}$$

$$\begin{aligned}h^{\mathrm{SB}_i}_{q,p}(t) = \sqrt{\frac{\eta_{\mathrm{SB}_i}}{K+1}} & \lim_{N_i \to \infty} \sum_{n_i=1}^{N_i} \frac{1}{\sqrt{N_i}} e^{j\left(\psi_{n_i} - 2\pi f_c \tau_{qp,n_i}\right)} \\ & \times e^{j2\pi f_{T\max} t \cos\left(\alpha^{(n_i)}_T - \gamma_T\right) \cos \beta^{(n_i)}_T} \\ & \times e^{j2\pi f_{R\max} t \cos\left(\alpha^{(n_i)}_R - \gamma_R\right) \cos \beta^{(n_i)}_R}\end{aligned} \tag{4b}$$

$$\begin{aligned}h^{\mathrm{DB}}_{q,p}(t) = \sqrt{\frac{\eta_{\mathrm{DB}}}{K+1}} & \lim_{N_1, N_2 \to \infty} \sum_{n_1, n_2 = 1}^{N_1, N_2} \frac{1}{\sqrt{N_1 N_2}} \\ & \times e^{j\left(\psi_{n_1,n_2} - 2\pi f_c \tau_{qp,n_1,n_2}\right)} \\ & \times e^{j2\pi f_{T\max} t \cos\left(\alpha^{(n_1)}_T - \gamma_T\right) \cos \beta^{(n_1)}_T} \\ & \times e^{j2\pi f_{R\max} t \cos\left(\alpha^{(n_2)}_R - \gamma_R\right) \cos \beta^{(n_2)}_R}.\end{aligned} \tag{4c}$$

Two vehicles are moving toward each other; thus, angles of arrival (AoAs) and angles of departure (AoDs) of LoS components are defined as: $\alpha_T^{\mathrm{LoS}} \approx \beta_T^{\mathrm{LoS}} \approx \beta_R^{\mathrm{LoS}} \approx 0$, $\alpha_R^{\mathrm{LoS}} \approx \pi$. $\alpha_{T/R}^{(n_i)}$ and $\beta_{T/R}^{(n_i)}$ are the azimuth and elevation (A/E) AoA(D) of the waves traveling from the effective scatterers $s^{(n_i)}$. Path delays for paths $Tx_p \to Rx_q$, $Tx_p \to s^{(n_i)} \to Rx_q$, and $Tx_p \to s^{(n_1)} \to s^{(n_2)} \to Rx_q$ are defined as τ_{qp}, τ_{qp,n_i}, and τ_{qp,n_1,n_2}, respectively. K designates the Rician factor, which indicates the power ratio of the LoS component to the non-LoS components. The Tx and the Rx are assumed to be moving at the speed of $\upsilon_{T/R}$ in the direction angle of $\gamma_{T/R}$, and $f_{T_{\max}}$ and $f_{R_{\max}}$ are the maximum Doppler frequencies with respect to the Tx and the Rx, respectively. In this model, $I = 3$, which means that there are three subcomponents for SB rays. These components correspond to the following: SB_1 denotes the reflection from the Tx sphere, SB_2 is the reflection from the Rx sphere, and SB_3 denotes reflections from the elliptic cylinder. Parameters η_{SB_i} and η_{DB} specify the amount of power that the SB and DB rays contribute to the total scattered power $1/(K+1)$, which satisfy $\sum_{i=1}^{I} \eta_{\mathrm{SB}_i} + \eta_{\mathrm{DB}} = 1$. The phases ψ_{n_i} and ψ_{n_1,n_2} are assumed to be independent and identically distributed random variables with uniform distributions over $[-\pi, \pi)$.

For DB reflections, there is no correlation between A/EAoD $(\alpha_T^{(n_i)}, \beta_T^{(n_i)})$ and A/EAoA $(\alpha_R^{(n_i)}, \beta_R^{(n_i)})$. However, for the SB reflection, they are related to each other based on a geometric relationship.

If all EAoDs and EAoAs are equal to zero as follows: $\beta_R^{\mathrm{LoS}} = \beta_T^{\mathrm{LoS}} = \beta_T^{(n_i)} = \beta_R^{(n_i)} = 0$ $(i = 1, 2, 3)$, the 3-D channel model becomes a 2-D model with two rings and one ellipse. In the following section, the different impacts of 3-D and 2-D channels on the BER performance will be investigated.

A. STCF

The space–time correlation function (STCF) property is investigated in this paper as it indicates the spatial correlation among subchannels. Such correlation has a significant impact on the performance of SM systems. Mathematically and under the assumption of wide-sense stationary, the STCF between any two complex fading envelopes $h_{qp}(t)$ and $h_{q'p'}(t)$ is defined as

$$\rho_{h_{qp}h_{q'p'}}(\tau) = \mathrm{E}\left[h_{qp}(t)h^*_{q'p'}(t-\tau)\right](K+1) \tag{5}$$

where $(\cdot)^*$ denotes the complex conjugate operation, and $\mathrm{E}[\cdot]$ is the statistical expectation operator. For this V2V channel model, the STCF is calculated as the superposition of correlation functions of the LoS component, SB components, and DB components as

$$\rho_{h_{qp}h_{q'p'}}(\tau) = \rho_{h_{qp}^{\mathrm{LoS}}h_{q'p'}^{\mathrm{LoS}}}(\tau) + \sum_{i=1}^{I} \rho_{h_{qp}^{\mathrm{SB_i}}h_{q'p'}^{\mathrm{SB_i}}}(\tau) + \rho_{h_{qp}^{\mathrm{DB}}h_{q'p'}^{\mathrm{DB}}}(\tau). \tag{6}$$

IV. Theoretical Average Bit Error Rate Analysis of Spatial Modulation Systems

The theoretical ABER of SM systems can be obtained via the union bound method [10], [17]–[21]. Referring to the upper bound presented in [10], we classify the errors into three categories: 1) error that only occurs in the digital modulation part with the probability $\underset{\mathrm{Signal}}{\mathrm{ABER}}$; 2) error that only occurs in the SM part with the probability $\underset{\mathrm{Spatial}}{\mathrm{ABER}}$; and 3) error that occurs in both parts with the probability $\underset{\mathrm{Joint}}{\mathrm{ABER}}$. The overall upper-bound expression of the BER is the combination of these three parts, which can be expressed as

$$\underset{\mathrm{SM}}{\mathrm{ABER}} \leqslant \underset{\mathrm{Signal}}{\mathrm{ABER}} + \underset{\mathrm{Spatial}}{\mathrm{ABER}} + \underset{\mathrm{Joint}}{\mathrm{ABER}}. \tag{7}$$

$\underset{\mathrm{Signal}}{\mathrm{ABER}}$ means the error only occurs in the digital modulation part, and the transmit antenna index is correctly detected. It is similar to the single-input–multiple-output case. The BER expression is given by

$$\begin{aligned}\underset{\mathrm{Signal}}{\mathrm{ABER}} &= \frac{1}{N_t}\frac{\log_2(M)}{m}\sum_{n_t=1}^{N_t}\underset{\mathrm{MOD}}{\mathrm{APEB}}(n_t) \\ &= \frac{1}{N_t}\frac{\log_2(M)}{m}\sum_{n_t=1}^{N_t}\frac{1}{M}\frac{1}{\log_2(M)}N_H(\chi\to\tilde{\chi})P(\chi\to\tilde{\chi}, n_t).\end{aligned} \tag{8}$$

In (8), $N_H(\chi \to \tilde{\chi})$ is the Hamming distance between modulated symbols χ and $\tilde{\chi}$, and $P(\chi \to \tilde{\chi}, n_t)$ denotes the pairwise error probability (PEP) that the transmitted symbol χ is detected as $\tilde{\chi}$. In (8), M is the modulation order; for example, if an M-PSK modulation scheme is used, (8) is given as [10], [17]

$$\begin{aligned}\underset{\mathrm{MOD}}{\mathrm{APEB}}(n_t) = \frac{1}{\log_2(M)}\sum_{l=1}^{M-1}\Bigg[\Bigg(&2\left|\frac{l}{M} - \left\lfloor\frac{l}{M}\right\rfloor\right| \\ &+ 2\sum_{k=2}^{\log_2(M)}\left|\frac{l}{2^k} - \left\lfloor\frac{l}{2^k}\right\rfloor\right|\Bigg)\Bigg]P_l(n_t)\end{aligned} \tag{9}$$

where

$$\begin{aligned}P_l(n_t) = &\frac{1}{2\pi}\int_0^{\pi\left[1-\frac{(2l-1)}{M}\right]} T_l^-(\theta, n_t)d\theta \\ &- \frac{1}{2\pi}\int_0^{\pi\left[1-\frac{(2l-1)}{M}\right]} T_l^+(\theta, n_t)d\theta\end{aligned} \tag{10}$$

$$T_l^-(\theta, n_t) = M_r\left(2\gamma\frac{\sin^2\left[\frac{\pi(2l-1)}{M}\right]}{\sin^2\theta}\right)$$

$$T_l^+(\theta, n_t) = M_r\left(2\gamma\frac{\sin^2\left[\frac{\pi(2l+1)}{M}\right]}{\sin^2\theta}\right). \tag{11}$$

In (11), γ is the signal-to-noise ratio (SNR), which can be defined as $\gamma = E_m/N$, where E_m is the transmit power, and N is the noise power. $M_r(.)$ is the moment-generating function (MGF) of $\sum_{n_r=1}^{N_R}\|h_{n_t,n_r}e\|^2$, where $e = \chi - \tilde{\chi}$. The closed-form expression of $M_r(.)$ is $M_r(s) = \prod_{i=1}^{N_R}(1 - s\lambda_i e)^{-1}$, where λ_i is the eigenvalue of the Rx correlation indicator matrix R_{Rx}. Similarly, we can define R_{Tx} as the correlation indicator matrix of the Tx. Considering this channel model, these two matrices are expressed as $R_{Tx}(p, \tilde{p}) = \rho_{h_{q,p}h_{q,\tilde{p}}}(0)$ and $R_{Rx}(q, \tilde{q}) = \rho_{h_{q,p}h_{\tilde{q},p}}(0)$, where $\rho_{h_{q,p}h_{q,\tilde{p}}}(.)$ is the STCF of the V2V channel model, which indicates the correlation between $h_{q,p}$ and $h_{q,\tilde{p}}$. As an ideal channel estimation is assumed at the RX side, $\tau = 0$.

For the case that the error only occurs in the SM part, which is expressed as $\underset{\mathrm{Spatial}}{\mathrm{ABER}}$ previously, we can refer to related investigations on space-shift keying (SSK) systems [18], [19]. This part can be expressed as

$$\underset{\mathrm{Spatial}}{\mathrm{ABER}} = \frac{1}{M}\frac{\log_2(N_t)}{m}\sum_{l=1}^{M}\underset{\mathrm{SSK}}{\mathrm{APEB}}(l). \tag{12}$$

$\underset{\text{SSK}}{\text{APEB}}$ can be further expressed as

$$\underset{\text{SSK}}{\text{APEB}}(l)=\frac{1}{N_t}\frac{1}{\log_2(N_t)}\times\sum_{n_t=1}^{N_t}\sum_{\tilde{n}_t=1}^{N_t}\left[N_H(n_t\to\tilde{n}_t)P(\kappa_l,n_t\to\tilde{n}_t)\right] \tag{13}$$

where $N_H(n_t\to\tilde{n}_t)$ is the Hamming distance between the antenna indexes n_t and $\tilde{n}_t$, and $P(\kappa_l,n_t\to\tilde{n}_t)$ is the PEP that the active antenna $\tilde{n}_t$ is detected given that n_t was transmitted with the modulation modulus κ_l. Referring to the ML detector algorithm in (2), this error can only occur when $\|y-h_{n_t,n_r}\kappa_l\|^2>\|y-h_{\tilde{n}_t,n_r}\kappa_l\|^2$. Thus, $P(\kappa_l,n_t\to\tilde{n}_t)$ can be written as

$$\begin{aligned}P(\kappa_l,n_t\to\tilde{n}_t)&=P\left(\|y-h_{n_t,n_r}\kappa_l\|^2>\|y-h_{\tilde{n}_t,n_r}\kappa_l\|^2\right)\\&=Q\left(\gamma\|h_{n_t,n_r}\kappa_l-h_{\tilde{n}_t,n_r}\kappa_l\|^2\right)\end{aligned} \tag{14}$$

where $Q(.)$ is the Q-function. Based on the alternative integral expression of the Q-function and the MGF-based approach [17], [20], (14) can be written as

$$P(\kappa_l,n_t\to\tilde{n}_t)=\frac{1}{\pi}\int_0^{\frac{\pi}{2}}M_{n_t,\tilde{n}_t}\left(\gamma\frac{\kappa_l^2}{2\sin^2\theta}\right)d\theta. \tag{15}$$

In (15), $M_{n_t,\tilde{n}_t}(.)$ is the MGF of $\sum_{n_r=1}^{N_R}\|h_{n_t,n_r}-h_{\tilde{n}_t,n_r}\|^2$, which can be expressed as $M_{n_t,\tilde{n}_t}(s)=\prod_{j=1}^{N_T}\prod_{i=1}^{N_R}(1-s\lambda_i u_j)^{-1}$, where u_j is the eigenvalue of the receiver correlation indicator matrix R_{Tx}. If constant modulus modulation schemes such as M-PSK are used, κ_l is a constant value as κ, and (12) can be simplified as

$$\begin{aligned}\underset{\text{Spatial}}{\text{ABER}}=\frac{1}{N_t m}\times\sum_{n_t=1}^{N_t}\sum_{\tilde{n}_t=1}^{N_t}\Bigg[&N_H(n_t\to\tilde{n}_t)\\&\times\frac{1}{\pi}\int_0^{\frac{\pi}{2}}M_{n_t,\tilde{n}}\left(\gamma\frac{k^2}{2\sin^2\theta}\right)d\theta\Bigg].\end{aligned} \tag{16}$$

For the third case, i.e., $\underset{\text{Joint}}{\text{ABER}}$, both digital modulation and SM parts are incorrect. It can be expressed as

$$\begin{aligned}\underset{\text{Joint}}{\text{ABER}}=\frac{1}{N_t M m}\sum_{n_t=1}^{N_t}\sum_{\tilde{n}_t\neq n_t=1}^{N_t}&\left[N_H\left(n_t,\chi\to\tilde{n}_t,\tilde{\chi}\right)\right.\\&\left.\times P\left(n_t,\chi\to\tilde{n}_t,\tilde{\chi}\right)\right]\end{aligned} \tag{17}$$

where $N_H((n_t,\chi)\to(\tilde{n}_t,\tilde{\chi}))$ is the Hamming distance for the error case that symbol χ transmitted by antenna n_t is detected as $\tilde{\chi}$ sent by antenna $\tilde{n}_t$, and $P((n_t,\chi)\to(\tilde{n}_t,\tilde{\chi}))$ is the corresponding PEP. Similar to the case of $\underset{\text{Spatial}}{\text{ABER}}$, it can be expressed as

$$\begin{aligned}P\left((n_t,\chi)\to(\tilde{n}_t,\tilde{\chi})\right)&=P\left(\|y-h_{n_t,n_r}\chi\|^2>\|y-h_{\tilde{n}_t,n_r}\tilde{\chi}\|^2\right)\\&=Q\left(\gamma\|h_{n_t,n_r}\chi-h_{\tilde{n}_t,n_r}\tilde{\chi}\|^2\right).\end{aligned} \tag{18}$$

Using the MGF-based approach, (18) can be represented as

$$P\left((n_t,\chi)\to(\tilde{n}_t,\tilde{\chi})\right)=\frac{1}{\pi}\int_0^{\frac{\pi}{2}}M_{n_t\chi,\tilde{n}_t\tilde{\chi}}\left(\frac{\gamma}{2\sin^2\theta}\right)d\theta. \tag{19}$$

In (19), $M_{n_t\chi,\tilde{n}_t\tilde{\chi}}(.)$ is the MGF of $\sum_{n_r=1}^{N_r}|h_{n_t,n_r}\chi-h_{\tilde{n}_t,n_r}\tilde{\chi}|^2$, with the expression of $M_{n_t\chi,\tilde{n}_t\tilde{\chi}}(s)=\prod_{j=1}^{N_T}\prod_{i=1}^{N_R}(1-s\lambda_i e u_j)^{-1}$.

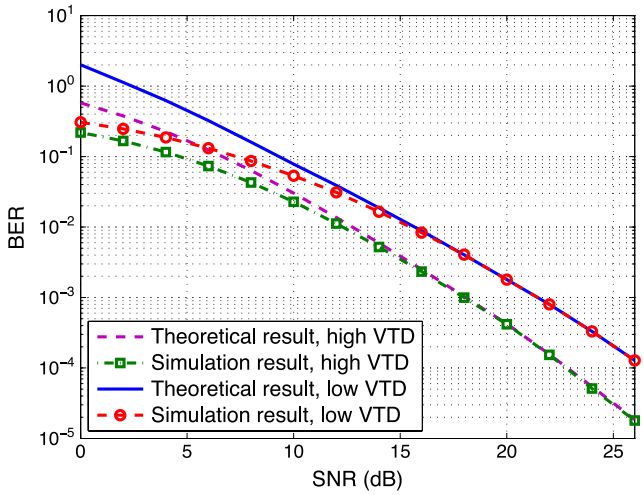

Fig. 1. Theoretical and simulated BER results of SM systems under the 3-D V2V MIMO channel model: a 2×2 system using the quaternary PSK (QPSK) modulation scheme.

V. Results and Discussions

Here, different simulation results are presented to evaluate the performance of SM systems under the 3-D V2V channel model. Based on the reported measurement in [22], the following key parameters are used to obtain these simulation results: $f_c=5.9$ GHz, $f_{T\max}=f_{R\max}=570$ Hz, the distance between the Tx and the Rx is $D=300$ m, $\gamma_T=\gamma_R=0^\circ$, and the space between two antenna elements is configured as 0.5λ. The K factors are configured as 3.786 and 0.756 for low- and high-VTD scenarios, respectively (see [7] for more details). All simulation results are obtained through Monte Carlo simulation; for each point in the following figures, the results of ten runs (each run transmits 100 000 symbols) are averaged to get the final value.

In Fig. 1, theoretical results of ABER for SM systems under the 3-D V2V channel model of different VTD scenarios are compared with simulation results. This figure indicates an excellent approximation of the theoretical derivation with simulation results, particularly in the high-SNR range, where SNR $\geq$ 15 dB. The theoretical ABER upper bound offers reasonable accuracy, which indicates the correctness of the theoretical derivation.

In Fig. 3, we investigated the performance of SM systems with different Doppler frequencies under both high- and low-VTD scenarios. First, it is noticed that a higher Doppler frequency will result in poorer BER performance. This phenomenon can be explained through Fig. 2, where the STCF of the channel model is shown. It can be observed that a higher Doppler frequency will result in faster fading, which increases the probability that the strength of signals is lower than the required threshold (high outage probability). Second, in Fig. 3, it is found that the SM system has better performance under the high-VTD scenario. Again, this can be explained with the help of Fig. 2, where it can be seen that under the high-VTD scenario, the correlation between subchannels is much lower than that under the low-VTD scenario. This is mainly caused by the difference of K factors for both scenarios. The higher K factor represents the stronger LoS component, which increases the spatial correlation among different channel paths. The high spatial correlation makes it difficult to determine which transmit antenna was active and degrades the performance [18]. Third, it is also observed in Fig. 3 that the SM system has better performance under the 3-D channel model. This can be also attributed to the lower spatial correlation of the 3-D channel as

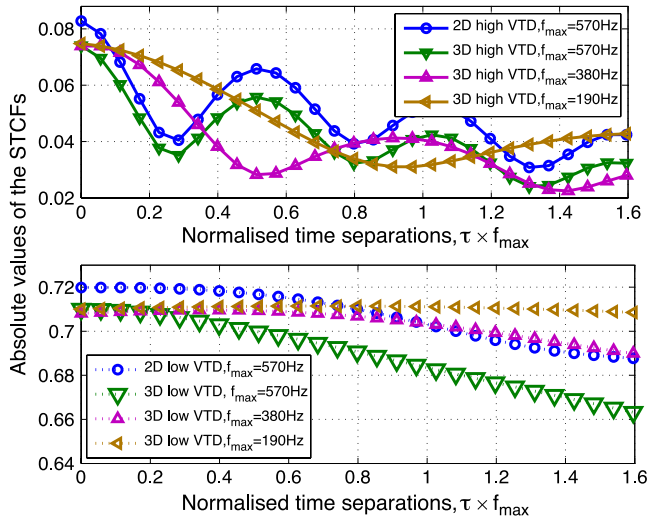

Fig. 2. Absolute values of STCFs for V2V MIMO channel models with different Doppler frequency and VTD scenarios.

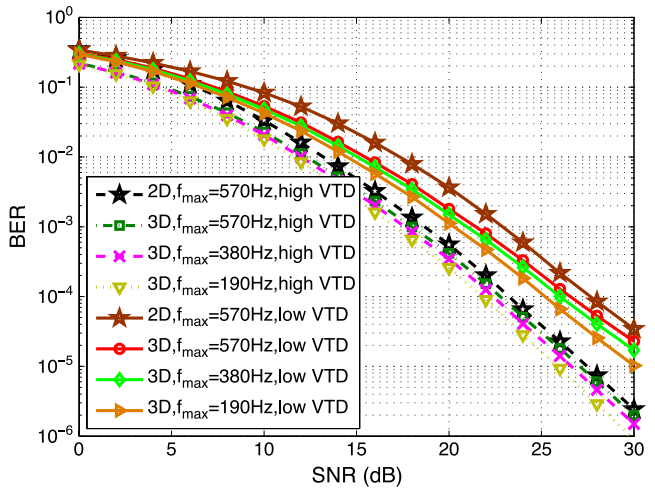

Fig. 3. BER performance of SM systems under the 3-D and 2-D V2V MIMO channel models with different Doppler frequency and VTD scenarios: a 2×2 system using the QPSK modulation scheme.

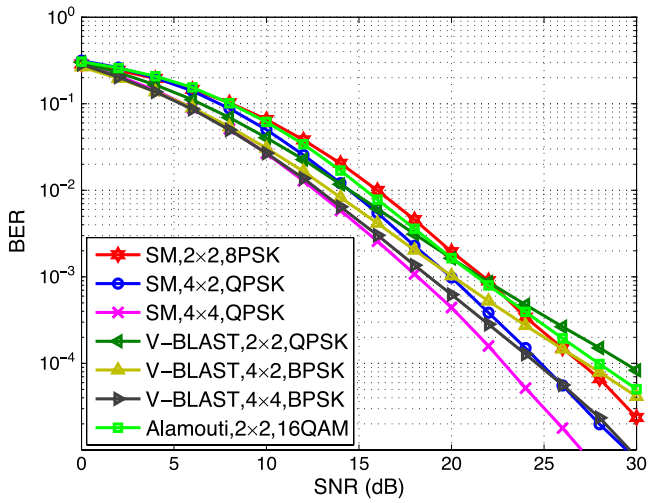

Fig. 4. BER performance of three different MIMO technologies under the 3-D V2V MIMO channel model for the high-VTD scenario, with the spectral efficiency of 4 bits/symbol.

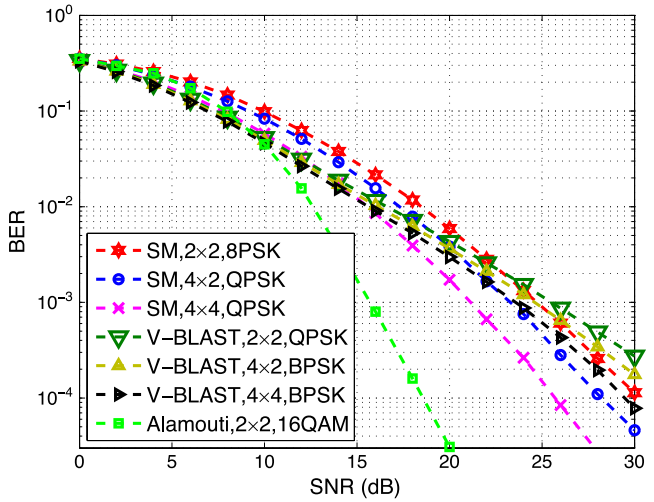

Fig. 5. BER performance of three different MIMO technologies under the 3-D V2V MIMO channel model for the low-VTD scenario, with the spectral efficiency of 4 bits/symbol.

compared with 2-D channel due to the extended vertical dimension. It is shown in Fig. 2 that the spatial correlation of the 3-D channel model is always lower than that of the 2-D model.

In Figs. 4–7, the SM system is compared with other MIMO technologies (V-BLAST and Alamouti scheme) under the 3-D V2V channel model of different VTD scenarios. Apart from VTD scenarios, different spectral efficiency values and system settings are also considered. For the V-BLAST system, ML is also employed as the receiver algorithm for a fair comparison. In Figs. 4 and 5, it is observed that for a 4-bit/symbol spectral efficiency and under a high-VTD scenario, the SM system using the 4×4 antenna setting obtains the best performance among all systems, particularly within the range of SNR $\geq$ 15 dB. Further investigating, the V-BLAST system can obtain a similar performance within the range of SNR $\leq$ 15 dB. Using the higher-order modulation scheme, the Alamouti scheme can still indicate good performance within the high-SNR range (SNR $\geq$ 14 dB) as a result of diversity gain. Under the low-VTD scenario, the Alamouti scheme shows significant performance enhancement due to the strong LoS component, whereas both SM and V-BLAST suffer from the high correlation among subchannels. However, compared with the V-BLAST system, the SM system demonstrates a 3-dB enhancement at the BER around 10^{-3}. In Figs. 6 and 7, similar comparisons are carried out with the spectral efficiency of 8 bits/symbol. Under both scenarios, the Alamouti scheme shows the worst performance due to using the higher order modulation scheme. The V-BLAST system can obtain similar or even better performance as the SM system within the range of SNR $<$ 14 dB, but the SM system is superior at the high-SNR range. However, when we use the ML receiver algorithm, the system complexity of V-BLAST is much higher than SM.

VI. Conclusion

In this paper, we have investigated the BER performance of SM systems under a novel 3-D V2V MIMO channel model. Numerical and simulation results have shown that the SM system has better performance under the high-VTD scenario due to the lower correlation

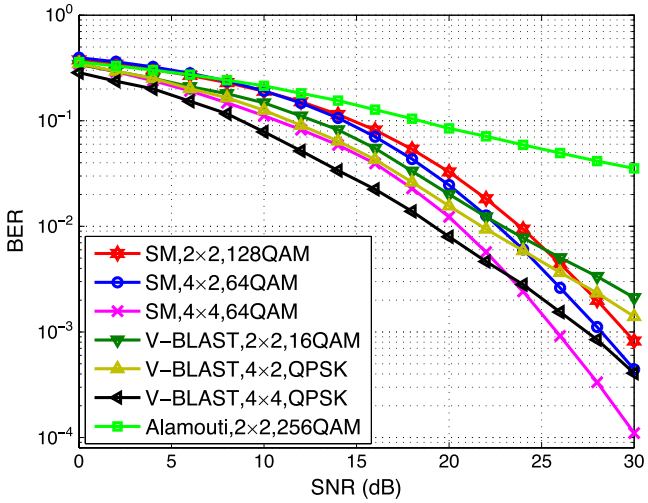

Fig. 6. BER performance of three different MIMO technologies under the 3-D V2V MIMO channel model for the high-VTD scenario, with the spectral efficiency of 8 bits/symbol.

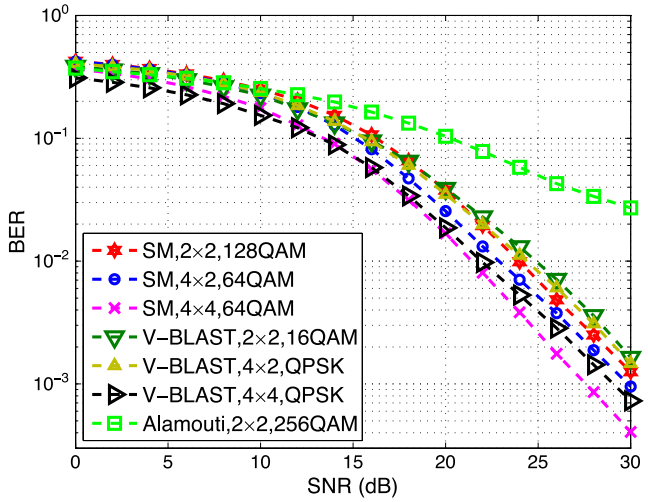

Fig. 7. BER performance of three different MIMO technologies under the 3-D V2V MIMO channel model for the low-VTD scenario, with the spectral efficiency of 8 bits/symbol.

between subchannels caused by weaker LoS components. A higher Doppler effect can result in worse BER performance due to higher outage probability. Additionally, SM systems can obtain better BER performance under the 3-D channel model than under the 2-D channel model due to the extended vertical dimension, which results in lower correlation of subchannels. When compared with other MIMO technologies, SM systems can yield an overall better tradeoff in terms of reliability, spectral efficiency, and system complexity.

REFERENCES

[1] C.-X. Wang *et al.*, "Cooperative MIMO channel models: A survey," *IEEE Commun. Mag.*, vol. 48, no. 2, pp. 80–87, Feb. 2010.

[2] R. Mesleh, H. Haas, S. Sinanovic, C. W. Ahn, and S. Yun, "Spatial modulation," *IEEE Trans. Veh. Technol.*, vol. 57, no. 4, pp. 2228–2241, Jul. 2008.

[3] M. D. Renzo, H. Haas, A. Ghrayeb, S. Sugiura, and L. Hanzo, "Spatial modulation for generalized MIMO: Challenges, opportunities, and implementation," *Proc. IEEE.*, vol. 102, no. 1, pp. 56–103, Jan. 2014.

[4] J. Jeganathan, A. Ghrayeb, and L. Szczecinski, "Spatial modulation: Optimal detection and performance analysis," *IEEE Commun. Lett.*, vol. 12, no. 8, pp. 545–547, Aug. 2008.

[5] J. Jeganathan, A. Ghrayeb, L. Szczecinski, and A. Ceron, "Space shift keying modulation for MIMO channels," *IEEE Trans. Wireless Commun.*, vol. 8, no. 7, pp. 3692–3703, Jul. 2009.

[6] C.-X. Wang, X. Cheng, and D. I. Laurenson, "Vehicle-to-vehicle channel modeling and measurements: Recent advances and future challenges," *IEEE Commun. Mag.*, vol. 47, no. 11, pp. 96–103, Nov. 2009.

[7] Y. Yuan, C.-X. Wang, X. Cheng, B. Ai, and D. I. Laurenson, "Novel 3-D geometry-based stochastic models for non-isotropic MIMO vehicle-to-vehicle channels," *IEEE Trans. Wireless Commun.*, vol. 13, no. 1, pp. 298–309, Jan. 2014.

[8] X. Cheng *et al.*, "Cooperative MIMO channel modeling and multi-link spatial correlation properties," *IEEE J. Sel. Areas Commun.*, vol. 30, no. 2, pp. 388–396, Feb. 2012.

[9] X. Cheng *et al.*, "Wideband channel modeling and ICI cancellation for vehicle-to-vehicle communication systems," *IEEE J. Sel. Areas Commun.*, vol. 31, no. 9, pp. 434–448, Sep. 2013.

[10] M. D. Renzo and H. Haas, "Bit error probability of SM-MIMO over generalized fading channels," *IEEE Trans. Veh. Technol.*, vol. 61, no. 3, pp. 1124–1144, Mar. 2012.

[11] A. Younis *et al.*, "Performance of spatial modulation using measured real-world channels," in *Proc. IEEE VTC Fall*, Las Vegas, NV, USA, Sep. 2013, pp. 1–5.

[12] J. L. Zhang, Y. Wang, L. Q. Ding, and N. T. Zhang, "Bit error probability of spatial modulation over measured indoor channels," *IEEE Trans. Wireless Commun.*, vol. 13, no. 3, pp. 1380–1387, Mar. 2014.

[13] N. Serafimovski *et al.*, "Practical implementation of spatial modulation," *IEEE Trans. Veh. Technol.*, vol. 62, no. 9, pp. 4511–4523, Nov. 2013.

[14] Y. Fu *et al.*, "A performance study of spatial modulation technology under vehicle-to-vehicle channel models," in *Proc. IEEE VTC Spring*, Seoul, Korea, May 2014, pp. 1–5.

[15] X. Cheng, C.-X. Wang, D. I. Laurenson, S. Salous, and A. V. Vasilakos, "An adaptive geometry-based stochastic model for non-isotropic MIMO mobile-to-mobile channels," *IEEE Trans. Wireless Commun.*, vol. 8, no. 9, pp. 4824–4835, Sep. 2009.

[16] X. Cheng, C.-X. Wang, B. Ai, and H. Aggoune, "Envelope level crossing rate and average fade duration of non-isotropic vehicle-to-vehicle Rician fading channels," *IEEE Trans. Intell. Transp. Syst.*, vol. 15, no. 1, pp. 62–72, Feb. 2014.

[17] M. K. Simon and M.-S. Alouini, *Digital Communication Over Fading Channels*, 2nd ed. Hoboken, NJ, USA: Wiley, 2005.

[18] M. Di Renzo and H. Haas, "Space Shift Key (SSK-) MIMO Over correlated Rician fading channels: Performance analysis and a new method for transmit-diversity," *IEEE Trans. Commun.*, vol. 59, no. 1, pp. 116–129, Jan. 2011.

[19] M. Di Renzo and H. Haas, "A general framework for performance analysis of Space Shift Keying (SSK) modulation for MISO correlated Nakagami-m fading channels," *IEEE Trans. Commun.*, vol. 58, no. 9, pp. 2590–2603, Sep. 2010.

[20] A. Hedayat, H. Shah, and A. Nosratinia, "Analysis of space–time coding in correlated fading channels," *IEEE Trans. Wireless Commun.*, vol. 4, no. 6, pp. 2882–2891, Nov. 2005.

[21] M.-S. Alouini and A. J. Goldsmith, "A unified approach for calculating the error rates of linearly modulated signals over generalized fading channels," *IEEE Trans. Commun.*, vol. 47, no. 9, pp. 1324–1334, Sep. 1999.

[22] G. Acosta and M. A. Ingram, "Six time- and frequency-selective empirical channel models for vehicular wireless LANs," *IEEE Veh. Technol. Mag.*, vol. 2, no. 4, pp. 4–11, Dec. 2007.